Journal of Ocean Engineering and Marine Energy
https://doi.org/10.1007/s40722-023-00292-z

CASE STUDY

Temporal upsampling of wave parameters and impact on time-domain floating body response and wave power

Hannah Mankle[1,2] · Paul Branson[3] · Bryony DuPont[1,2] · Bryson Robertson[2,4]

Received: 12 April 2023 / Accepted: 5 July 2023

Abstract
Power production of wave energy converters (WEC) predicted in the time domain use wave resource parameters and time-domain hydrodynamic model simulations that provide high temporal resolutions (10s of Hz). However, wave resource parameters are often based on frequency-domain calculations with temporal resolution of 30 min to an hour. Real ocean wave conditions vary on much shorter time scales. Relying on frequency-domain calculations will not be sufficient to capture short-term variability and accurately predict WEC power production for a standardized methodology that follows power system requirements. Low temporal resolution data sets are being used in a majority of studies to generate representative wave conditions as inputs to numerical simulations by generating wave spectra. Spectra are then used to predict the efficiency of systems that will not accurately capture the variability of waves in short timeframes. Creating a standardized methodology to increase the temporal resolution of metaocean conditions to inform model development can provide better power production forecasting. In this paper, random amplitude, Fourier coefficient methods have been used for WEC simulations of finite durations to improve the observed variability in wave heights and power production. Variability using this method does increase for finite durations compared to the commonly used deterministic amplitude method.

Keywords Temporal sampling · Wave energy · Time-domain modeling

1 Introduction

Marine renewable energy resources provide an opportunity to incorporate clean, sustainable, and reliable energy in applications that have traditionally relied on fossil fuel electricity generation, such as grid scale electricity, desalination, ocean observation and monitoring, and aquaculture. Much like traditional variable renewable technologies—specifically wind and solar—marine renewable energy technologies need reliable forecasting information at a variety of temporal resolutions to operate efficiently and effectively (Ren et al. 2015; Reikard and Rogers 2011). In addition, forecasting is critical for grid-scale power development, as marine renewable energy technologies generate intermittent power, and as such, may require smoothing or back-up resources to allow integration into the larger grid. Smaller, distributed electricity systems will be even more sensitive to the inclusion of marine renewable energy in the mix, as stochasticity in the wave resource contributes to variability in the generation of power by marine renewable energy systems. At both the grid scale and distributed systems, it is unclear how variability in the ocean resource should be implemented to model and predict power generation accurately. There is a pressing need to characterize the variability of ocean waves at shorter time periods (< 30 min) to provide this insight (Said and Ringwood 2021).

The prediction of wave conditions, or forecasting, provides weather and sea conditions for many types of marine applications (such as shipping, fisheries, and ocean recreation), with typical numerical prediction methods estimating conditions days in advance. Currently, the data used to inform these prediction methods is either modeled or collected using

✉ Bryson Robertson
bryson.robertson@oregonstate.edu

1 Mechanical, Industrial, and Manufacturing Engineering, Oregon State University, Corvallis, OR 97330, USA

2 Pacific Marine Energy Center, Oregon State University, Corvallis, OR 97330, USA

3 Coasts and Ocean Research Program, Commonwealth Scientific and Industrial Research Organisation, Crawley, WA 6009, Australia

4 Civil and Construction Engineering, Oregon State University, Corvallis, OR 97330, USA

Published online: 28 July 2023

ocean sensors; the collected data may be limited by the temporal resolution, as most available wave data have been averaged over at least 20 min and sampled hourly (National Oceanic and Atmospheric Adminitration 2022). While this hourly resolution of wave data satisfies the numerical wave forecasting needs of many marine applications, hourly resolution is likely too coarse to be useful in the burgeoning marine energy and blue economy sectors—particularly in situations, where power production must be predicted on short time scales to maintain system reliability (Rojas and Rousan 2017). The large variability and stochasticity of ocean waves in very short time periods—and therefore, the variation in power production of wave energy systems due to this stochasticity is not captured in averaged wave data sampled at hourly time intervals (Tucker et al. 1984; Saulnier et al. 2009; Mérigaud and Ringwood 2018).

Simulations of wave energy converter (WEC) hydrodynamic performance require high-temporal-resolution free-surface inputs. Currently, the generation of free-surface time-series for WEC numerical modelling often uses publicly available wave data, based on 30-min to 1-h averaging intervals (within this work, averaging interval is used to define the temporal time steps used to calculate representative wave parameters). Using 30-min to 1-h intervals to generate these representative free surface conditions in WEC modelling reduces the natural variation in wave height, as the longer time averaging intervals smooths over any short-term variability (Tucker et al. 1984; Mérigaud and Ringwood 2018). Decreasing the averaging interval will better represent the natural variation of a ocean conditions and the associated time series generated for the wave resource.

A practical challenge with wave measurements is access to high-temporal-resolution data. Most of the numerical modeling currently used for WEC simulations uses wave measurements with averaging intervals of 30 min to 1 h, or phase-averaged numerical wave model hindcasts with output intervals of 3 h. Examples include the National Oceanic and Atmospheric Adminitration (2022) National Data Buoy Center historical archive, the Coastal Data Information Program University of California, the Department of Energy Water Power Technology Office (2023) US Wave Data Set, the European Center for Medium-Range Weather Forecast (Medium-Range Weather Forecasts 2023; OceanSITES 2023), and the Australia Ocean Data Network (2023).

Using wave data with large averaging intervals can misrepresent the true variability in the ocean conditions. For example, 1-h averaging intervals produce representative free-surface elevation data that removes the variability over shorter time intervals. This leads to a misrepresentation of the wave field that a WEC will encounter and a decrease in the representation of extreme values. Thomson et al. (2016) quantify this misrepresentation when calculating statistical parameters using 10-min sample periods of high temporal resolution measured free-surface time series. Specifically, they discovered that extreme wave height conditions, identified using 10-min averaging intervals, would be obscured if representing the time series using hourly-averaged wave parameters. Current methods for generating free-surface time series for WEC simulation use 1-h averaging intervals to produce the representative time series with the deterministic amplitude scheme to analyze performance metrics of WECs (Tucker et al. 1984; Mérigaud and Ringwood 2018). As in Thomson et al. (2016), variation of the waves is significantly lowered when using this common method. Further details on wave modeling methods for WEC simulation and the impact of varying time resolutions on wave parameters and WEC design will be discussed in Sects. 2.1 and 2.2.

The International Electrotechnical Commission (IEC) technical specification 62600-101 (IEC 2015) encourages the use of measured or modeled wave data to represent wave conditions at a given site. Specifically, the IEC strongly suggests numerical analysis using 10 years of wave data with temporal resolutions of 3 h for the reconnaissance and feasibility resource assessment classes. The highest threshold in the technical specification for the design of wave energy converters requires an hourly temporal resolution while capturing the meteorological variability in average wave conditions does to capture the stochasticity of water surface elevation at shorter timescales, this is too coarse to observe the natural free-surface elevation changes and provide realistic WEC power variability predictions.

The objective of wave data upsampling is to generate free-surface water elevation time series that provide statistically representative wave heights over short averaging intervals to forecast performance and reliability metrics for marine renewable energy technology and offshore platforms. Currently, computational cost and memory constraints limit the direct application of common short-term phase resolved wave forecasting models over large geographic regions. There is a distinct need for a low computational cost representative method to provide temporally upsampled wave parameters. As such, the novel method introduced in this paper was constrained by the need to have reduced computational cost and have reduced input data needs to develop probabilistic free-surface time series.

This paper presents a novel methodology to increase the temporal resolution of commonly available wave parameters, via a phase-resolved upsampling approach. Section 2 includes a background on wave parameterization and the current modeling practices for wave energy technologies. Section 3 describes the upsampling methodology we investigated. Section 4 provides overviews of the case studies conducted in this paper. Section 5 shows the results of this study, followed by the discussion and conclusion in Sects. 6 and 7.

2 Background

Renewable energy resource predictions, for different averaging intervals, are either based on phase-averaged or phase-resolved methods. It is commonly understood that phase-resolved models have higher accuracy for short-term horizons, due to the dependence between time steps (Ren et al. 2015), while phase-averaged models have higher accuracy for longer forecasting windows.

In the analogous field of wind energy, the length of time into the future for which forecasts are prepared are categorized as: (1) very-short-term, with averaging intervals under 30 min; (2) short-term, with averaging intervals between 30 min and 6 h; (3) medium-term, with averaging intervals between 6 and 24 h; or (4) long-term, with averaging-intervals greater than 24 h (Ren et al. 2015). Wave predictions also follow this forecasting horizon categorization and forecasting methodologies (Reikard et al. 2015).

The varying forecast horizons all have dedicated uses for grid applications. Shorter intervals provide necessary power information to utility operators, allowing them to adjust the grid generation and demand based on the intermittent resources. Medium-to-long-term intervals provide longer forecasting windows which are useful for operational and maintenance planning. The focus in this study is on characterizing the variability in predicted wave resources by employing very-short-term forecasting with intervals below 30 min.

2.1 Wave modeling methods

Phase-averaged wave methods (or time-averaged methods) model changes in the frequency domain wave spectrum. Third-generation wind-wave models such as SWAN (team TS 2018), WAM (Group TW 1988), and WAVEWATCH-III (Tolman 2009) are examples of phase-averaged models (Robertson 2017). These models are used to conduct hindcasts, evaluate wave energy resources, and forecast ocean wave conditions.

For phase-averaged models, the statistical properties of the waves are assumed constant within the averaging interval, i.e., assuming the wave spectra are stationary in space and time over the 1–3 h interval used to develop the spectrum. Spectra are created using wave elevation measurements averaging over a sufficiently large number of waves, leading to higher accuracy for medium-to-long forecasting horizons with longer averaging intervals. Examples of wave spectral shapes include the Pierson–Moskowitz (PM) (Pierson and Moskowitz 1964) and JONSWAP (Hasselmann et al. 1973) spectra. The PM, for example, characterizes a fully developed sea, where the wind-generated waves have propagated over a significantly long distance. The JONSWAP spectrum characterizes a developing sea by adding a spectral shape parameter to the PM spectrum to represent the steepness of the sea.

Phase resolved wave inputs for numerical modeling of offshore systems can vary in complexity and generally fall into two categories: regular and irregular waves. Unidirectional monochromatic waves—or regular waves—are low-complexity waves often used for early design work and used for benchmark validation of numerical models against experimental testing (Alves 2016). Irregular phase-resolved methods (or time-resolved methods) allow for accurate short-term deterministic predictions of water elevation characteristics. Capturing the stochastic nature of the water elevation, and associated waves, for very-short time periods will aid in the design, operation, and survivability of marine infrastructure and technologies. Survivability of WEC systems is paramount for the implementation of these technologies into marine applications which further highlights the need for short-term forecasting and proper wave representative models.

Wave stochasticity introduced in time-resolved methods provides a more realistic realization of the free surface variance. Phase-resolved free-surface elevation data are directly measured or recreated through an inverse Fourier analysis of spectra from a phase-averaged model.

Irregular wave inputs allow the numerical model to simulate the WEC hydrodynamic interactions by generating elevation time series based on the linear superposition of regular waves. One common method of modeling irregular waves takes the significant wave height and peak period to calculate the wave spectral density using either a JONSWAP, PM, or Bretschneider spectral shape (Ricci 2016). Historical publicly accessible data is often used to inform irregular wave inputs, i.e., to simulate WECs in high energy waves.

A common method for generating a free-surface, or phase resolved, time series for WEC simulation is the deterministic amplitude scheme (DAS) (Tucker et al. 1984; Mérigaud and Ringwood 2018; Saulnier et al. 2009). In the DAS, harmonic sinusoidal wave components are summed with random phases and spectrum-derived amplitudes. DAS generates a time series from power spectra with phases (ϕ_k) chosen randomly over a uniform-distribution from $[0; 2\pi]$. The deterministic free-surface elevation time series equation η_{t_i} for a given spectral density function $S(f)$ of a finite length $T = N\Delta t$ can be expressed as follows:

$$\eta_{t_i} = \sum_{k=1}^{M/2} A_k \cos\left(2\pi f_k t_i + \phi_k\right), \tag{1}$$

with the ith and kth elements $i = 1 \ldots N$ and $k = 1, \ldots, M/2$, where $M/2$ is the number of discrete frequency components (typically $M = N$). In addition, the timestep $t_i = N\Delta t$, frequency $f_k = k\Delta f$, where $\Delta f = \frac{1}{M\Delta t}$,

and amplitude $A_k = \sqrt{2\,S(f_k)\Delta f}$. Unless the simulation time is trending towards infinity with a constant time step, DAS will generate time series with the same spectral shape and variance (Mérigaud and Ringwood 2018). This results in similar spectral moments and significant wave heights for each realization. For realistic free-surface time series, each realization should vary from the mean, especially as the averaging-interval decreases.

A second phase-resolved method, random amplitude scheme (RAS) assigns two amplitude components randomly, based on a Gaussian distribution with a variance given by the spectral density function (Tucker et al. 1984; Mérigaud and Ringwood 2018; Saulnier et al. 2009). RAS realistically reproduces the characteristics of a Gaussian process to generate free-surface time series, which is described in Eq. 2:

$$\eta_{t_i} = \sum_{k=1}^{M/2} a_k \cos\left(2\pi f_k t_i\right) + b_k \cos\left(2\pi f_k t_i\right) \tag{2}$$

$$A_k = \sqrt{a_k^2 + b_k^2}, \tag{3}$$

where the amplitudes a_k, b_k are chosen randomly, with an assigned seed, following a normal distribution with a standard deviation of $\sqrt{S(f_k)\Delta f}$ and a mean of zero.

Note that Eqs. 1 and 2 are equivalent. The relationship between a_k, b_k and A_k can be found in Eq. 3. When using Eq. 1 for the RAS, the phase is chosen randomly, following a uniform distribution from $[0; 2\pi]$. A_k is randomly selected following a Rayleigh distribution with a variance of $2S(f_k)\Delta f$.

It is important to note that in the RAS, significant wave height will vary from the mean for each realization to better represent a realistic time series. If both RAS and DAS are used to generate multiple time series with similar input parameters, DAS will produce a significant wave height close to the mean of the realizations generated using RAS. Given the widespread use of DAS, a comparison of the spread of H_s is explored in Sect. 5. A more in-depth discussion on the advantages and disadvantages of using DAS and RAS can be found in Mérigaud and Ringwood (2018).

2.2 Impact of different time resolutions on wave parameters and WEC design

Designing marine infrastructure requires extensive knowledge about how the structures will interact with the waves. Establishing wave forecasting models, especially for short averaging intervals, provides opportunities for increased structural reliability modeling and more realistic wave interaction modeling. The total uncertainty surrounding WEC performance is difficult to quantify given the complexity inherent in the ocean and the wide variety of WEC archetypes. Specific to wave representation, the most common method for wave inputs, DAS, entails using inverse fast Fourier transform (FFT) to calculate the spectrum needed to generate the time series. However, this methodology neglects the stochastic nature of waves and only preserves the spectral moments of the spectral density function at individual realizations.

Mérigaud and Ringwood (2018) recommend the use of DAS for long-term WEC analysis and recommend RAS for short-term analysis. They note that DAS' performance is limited for short-term forecasting due to the random variable statistical representation and associated performance variability that lead to inaccurate WEC power assessments. However, when calculating long-term average power performance, DAS only requires one simulation to achieve the average, where RAS would require more simulations to achieve the same mean with small error.

Ricci et al. (2008) explore different time-domain methods to estimate the dispersion of mean power in a simple single-body point absorber WEC and follow the methodology for RAS and DAS established in Tucker et al. (1984). They analyzed simulations of different durations and discover the duration has a strong influence on the statistical dispersion of the average power. As duration decreases, the power variation increases but the average power value for all durations remain the same.

Saulnier et al. (2009) investigate the mean power performance of DAS and RAS time-domain representations. They find the absolute value of extracted power, the duration of the simulation, and the spectral bandwidth all influence the precision of power estimation. RAS and DAS result in similar average absorbed power but the standard deviation of power using DAS was consistently lower than when RAS was used.

Although RAS provides a significant improvement for the statistical wave representation, DAS remains the most commonly used form of wave representation. One research area more frequently adopting the application of RAS is WEC control research. Examples of the use of RAS for control strategy development can be found in Fusco and Ringwood (2010), Peña-Sanchez et al. (2020), and Gioia et al. (2022). Short-term forecasting is of great interest for developing advanced control strategies.

A number of other authors have focused on improving the numerical modeling accuracy of WEC performance and the need for higher temporal resolution. Reikard et al. (2015) investigate the grid integration of WEC arrays by exploring the spatial and temporal resolution. They conclude that multiple arrays placed, where wave resources vary significantly can help smooth the variability of the total power and provide a more predicable output. Fairley et al. (2017) observe a more predictable and smooth power performance when placing WEC arrays in multiple sites across the UK. The smallest forecasting horizon in both these studies are hourly, which

leads to an under-representation of the true power variability for each array if forecasting very-short horizons.

Robertson et al. (2021) provide an upsampling strategy to increase temporal resolution to assess WEC agnostic power performance by generating time series from power density spectra of averaging intervals from 5 to 30 min. They show an increase in WEC power variability for very-short averaging intervals while maintaining consistent annual mean and total energy values. However, the upsampled time series were produced using DAS which does not produce accurate statistical and extreme value representation.

2.3 Common wave energy converter modeling methods

2.3.1 Frequency-domain modeling

Modeling WECs in the frequency domain is a computationally inexpensive method that calculates the device hydrodynamics and responses as a linear function of frequency. Hydrodynamics and responses are calculated using linear potential flow solvers and boundary element method codes, such as Capytaine (Ancellin and Dias 2019), Nemoh (Babarit and Delhommeau 2015), and WAMIT (Tobergte and Curtis 2013).

The governing equation of motion in the frequency domain is

$$-\omega^2 m\ddot{X}(\omega) = F_{\text{ex}}(\omega) + F_{\text{rad}}(\omega) + F_{\text{hs}}(\omega) + F_{\text{PTO}}(\omega) + F_m(\omega), \quad (4)$$

$$F_{\text{PTO}}(\omega) = i\omega B_{\text{PTO}}\dot{X}(\omega) - K_{\text{PTO}}X(\omega), \quad (5)$$

$$F_m(\omega) = -K_m X(\omega), \quad (6)$$

where m is the mass of the system, $\ddot{X}$ is the acceleration of the body and F is the sum of the external and reaction forces acting on the body. The external loads include the hydrostatic force, F_{hs}, due to the variation of the hydrostatic pressure distribution; excitation force, F_{ex}, due to the interaction between the incident waves against a static geometry; and radiation force, F_{rad}, due to the change in momentum of the fluid from the motion of the geometry. The linear reactionary power-take-off (PTO) force, F_{PTO}, is caused by the controllable reaction force from the PTO system. B_{PTO} and K_{PTO} in Eq. 5 are the damping and spring coefficients. The mooring force, F_m, arises from a constraint set on the WEC to hold it in position with a spring stiffness K_m. Nonlinear interactions, often associated with large or extreme wave conditions, will not be represented accurately in the frequency domain. For further detail on the frequency-domain method, refer to Alves (2016) and Bosma et al. (2012).

2.3.2 Time-domain modeling

Frequency-domain modeling using linear forcing is a good early design methodology, but a WEC system must capture the nonlinearities to incorporate complex PTO configurations, viscous drag, and other nonlinear interactions to simulate more realistic models. This is crucial for future grid integration and complex wave to wire studies (Said and Ringwood 2021). Expanding on Eqs. 4, 7 describes the forces accounted for in the time domain:

$$(M + A_\infty)\ddot{X}(t) = F_{ex}(t) + F_{rad}(t) + F_{PTO}(t) + F_{drag}(t) + F_{hs}(t) + F_m(t), \quad (7)$$

where M is the mass matrix, A_∞ is the added mass, and F_{drag} is the damping force accounting for viscous losses. Added mass, wave excitation force, and radiation are taken straight from the frequency-domain model. Ricci (2016) and Babarit et al. (2011) have further details on the time-domain modeling process.

Power generated for linear a PTO system, as is the case in the WECs used in this paper, are modeled as a spring-damper system:

$$P_{\text{PTO}}(\omega) = -F_{\text{PTO}}\dot{X}_{\text{rel}} = K_{\text{PTO}}X_{\text{rel}}\dot{X}_{\text{rel}} + B_{\text{PTO}}\dot{X}^2_{\text{rel}}, \quad (8)$$

where X_{rel} and $\dot{X}_{rel}$ are the relative position and velocity of a WEC. The time-domain software used in this paper is the open-source software WEC-Sim, further detail on the theory can be found in the software documentation (Ruehl et al. 2022).

2.4 Resource assessment and power performance metrics

Three common metrics for representing WEC power performance include power matrices, mean annual energy production (MAEP), and seasonal power variation. All these methods require at least 10 years of wave data per IEC TS 62000-100 (2012) and a thorough understanding of the wave resource characteristics of an intended location. Power matrices are often used to represent the amount of power a WEC will produce for an irregular wave field with a specific significant wave height and energy period. These matrices provide information on the occurrence and power of the system within the H_s and peak period, T_p bins. To calculate the MAEP, each bin in the power matrix is multiplied by its annual occurrence and summed together. Short-term power metrics focus more on the power production of the simulated time series. This includes and is not limited to the average power, maximum power, peak-to-average power ratio, and the coefficient of variation of power.

3 Methodology

The theory behind our probabilistic model used to generate a time series is discussed in Sect. 3.1. Section 3.2 discusses the practical implementation of the process as an input into WEC-Sim or other time-domain hydrodynamic models.

3.1 Free-surface time series generation theory

To achieve a realistic representation of the influence of the stochastic random wave field on the power generation, we conducted 10-million-member ensemble Monte-Carlo simulation using the RAS method and linear wave theory (Eq. 2). The resulting time series, $\eta(t)$, are analyzed in the time-domain using zero-down crossings to identify individual waves and in the frequency-domain for spectral parameters. For each time series, the random seed is retained, and the following wave parameters are calculated: significant wave height (H_s), maximum wave height ($H_{\max}$), mean zero-crossing period (T_z), and the crest to trough correlation (r). For the purposes of this paper, we focus on the probabilities of H_s, $H_{\max}$, and their effect on the performance metrics of two WECs and an offshore wind platform. Further details on the different case WECs and floating offshore wind platform are found in Sect. 4.

In total a 10-million-member ensemble of time-series are analyzed and random seeds corresponding to specific percentiles in the distributions of H_s and $H_{\max}$ identified. This allows the regeneration of time-series in particular regions of the empirical single- and joint-probability distributions. The distributions are a function of the number of waves (proxy metric representative of averaging interval) and the spectral peak enhancement factor, γ. Using linear wave theory, distributions are created using parameters with a value of 1 and can be by scaled by H_s and T_p. Equations 9–13 describe the Pierson–Moskowitz (PM) and JONSWAP spectrum with γ, normalized frequency $\hat{f} = \frac{f}{f_p}$, and $f_p = \frac{1}{T_p}$:

$$S_{PM}(\hat{f}) = \frac{H_s^2}{3.2 f_p} \hat{f}^{-5} exp(-1.25\hat{f}^{-4}), \tag{9}$$

$$S_J(\hat{f}) = C_J . S_{PM}(\hat{f}) . \gamma^{-\frac{(\hat{f}-1)^2}{2\sigma^2}}, \tag{10}$$

$$C_J = \frac{H_s^2}{16 m_0}, \tag{11}$$

$$m_0 = \int_0^\infty S_{PM}(\hat{f}) . \gamma^{-\frac{(\hat{f}-1)^2}{2\sigma^2}} \, d\hat{f}, \tag{12}$$

$$\sigma = \begin{cases} \sigma_a & \text{for } \hat{f} \leq 1 (\text{typically} : 0.07) \\ \sigma_b & \text{for } \hat{f} > 1 (\text{typically} : 0.09), \end{cases} \tag{13}$$

where C_J is a scaling coefficient for the JONSWAP spectra calculated by integration that accounts for the peak enhancement factor. For fully developed seas, γ is 1, simplifying the JONSWAP spectrum to the Pierson–Moskowitz spectrum. The spectra being calculated using the RAS method are kept at a constant high-resolution ($M = 2^{16}$) for all averaging intervals to prevent biasing of the time series variance due to differing sampling intervals (i.e., FFT-length). If the time series output is longer than the averaging interval it was truncated to the desired averaging interval. Figure 1 shows the flowchart of the simulation process, focusing on the wave input generated with the probabilistic model.

Free surface time series, $\eta(t)$, simulation inputs are then regenerated from the stored random seeds at designated percentiles and scaled to a specific H_s and T_p. The range of values for T_p is dependent on location but will typically be between 6 and 20 s. The averaging interval is determined by multiplying the number of waves by the peak period, e.g., a time series with 20 waves and a T_p of 10 s will have an averaging interval of 200 s.

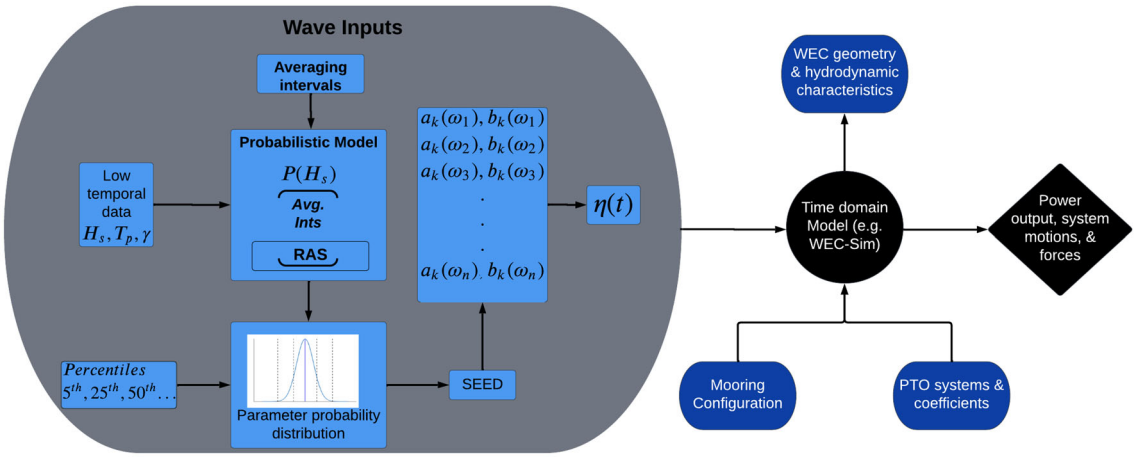

Fig. 1 Flowchart of the time-domain modeling process for a WEC with a focus on the wave input and the generation of a wave time series, $\eta(t)$, based on an upsampled probabilistic model

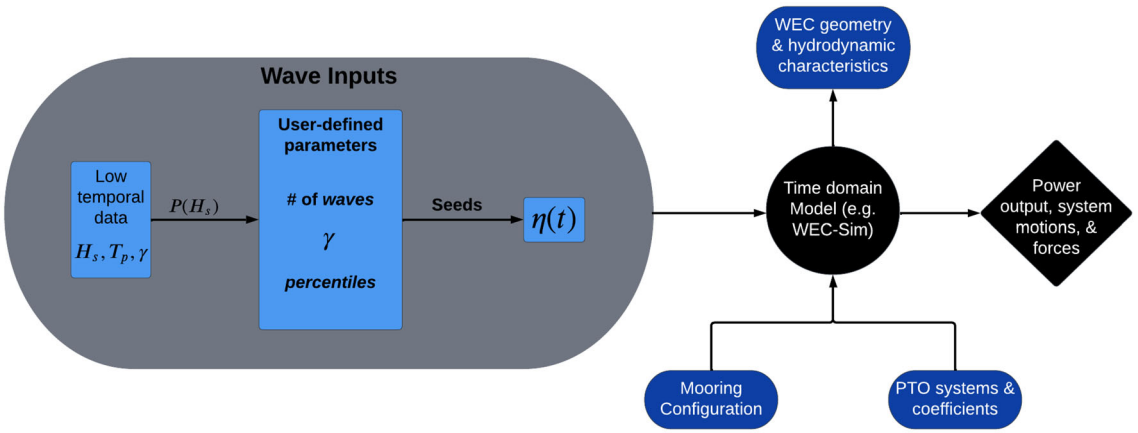

Fig. 2 Flowchart of the time-domain modeling process for a WEC with a focus on the wave input, $\eta(t)$, and the generation of a wave time series based on an upsampled probabilistic model

3.2 Free-surface time series implementation

Once the empirical probability distributions have been identified, the implementation into time-domain modeling is straightforward. As shown in Fig. 2, the user-defined parameters are averaging interval (in minutes), spectrum peak enhancement factor (γ), and the distribution percentile. The pre-calculated distribution percentiles include 5th, 25th, 50th, 75th, and 95th percentile.

The size of the probabilistic model, spanning all percentiles and realizations, is large and would dramatically increase the computational time of the upsampling methodology. As such, choosing specific percentiles spanning the distribution is sufficient for forecasting possible wave conditions for WECs.

4 Methodology case study

4.1 Wave resource

The upsampling methodology will be demonstrated using information and data from the PacWave South open-ocean wave energy test site off the coast of Newport, Oregon, USA PacWave (xxxx). PacWave is a grid-connected, 20 MW, 4-berth test facility that is being developed in partnership with the US Department of Energy, the State of Oregon, Oregon State University (OSU) and local stakeholders. As a result, the pacific northwest of the US will provide significant opportunities for future wave and offshore wind energy development due to PacWave and the active wave/wind climate. Figure 3 shows the location of PacWave South facility.

Initially, to validate the methodology, the variability of the upsampling method free-surface time series is compared against high resolution wave measurements collected near the PacWave South test site. Wave data were collected from surface wave instrument floats with tracking (SWIFT) buoys in 2016 (Thomson 2012). The SWIFT buoys have a sample frequency of 25 Hz and take measurements in 10-min bursts. A more detailed description of the SWIFT capabilities and specifications can be found in Thomson (2012). Due to the free-floating nature of SWIFT buoys, the same assumptions are used in Thomson et al. (2016), where the wave statistics are calculated as stationary.

4.2 WEC and floating offshore wind technology case studies

Investigating and validating the proposed methodology is essential for the hydrodynamic response and performance metrics of different floating offshore technologies. The probabilistic model used in the upsampling process has constant distributions of wave parameters, regardless of the location chosen. The normalized distributions are linearly adjusted based on the wave parameters of choice, averaging interval, and percentiles input into time-domain models. However, given the non-linear nature of wave–body interactions, the probabilistic distributions of wave conditions cannot directly inform the response or performance of the floating technologies under these improved methods.

In the following sections, two different size WECs are introduced to investigate the impact of the upsampled free-surface time series on the performance of the WECs. A third case examines how the upsampled time series effects the surge force acting on a semi-submersible floating wind platform; which has direct implications for mooring and anchoring system design. Providing accurate forecasts, with very-short averaging intervals, provides more detail on the hydrodynamic–structural interactions which can be used for structural response and reliability models.

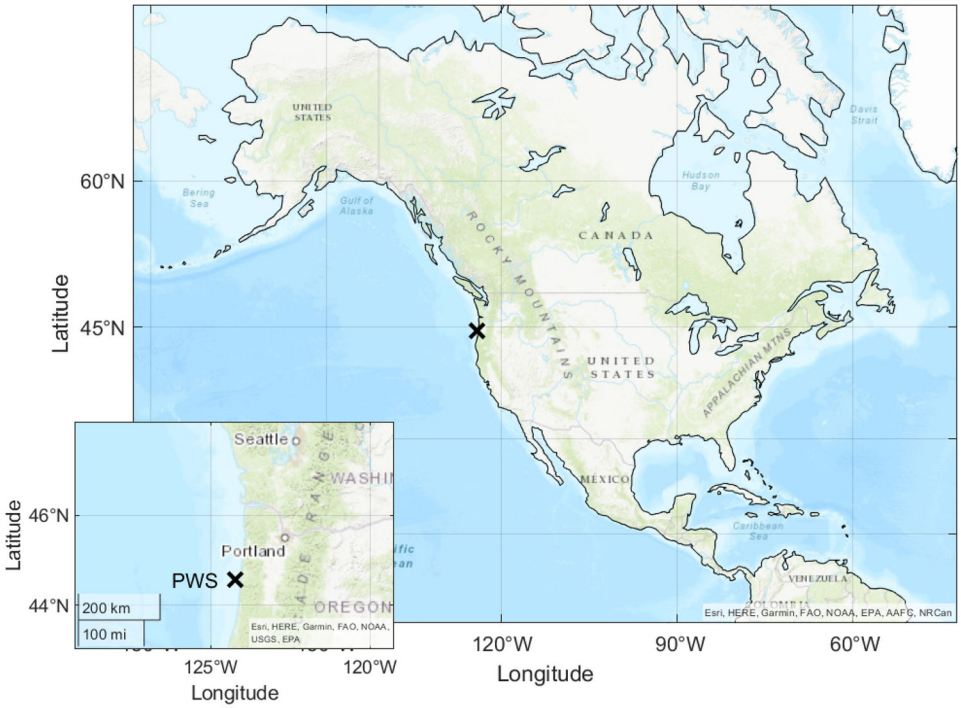

Fig. 3 Map of the Oregon coast, displaying the location of PacWave South test site. SWIFT buoys collected the high resolution wave measurements just North of PWS and were free drifting, with the path moving North

LUPA	MiniWEC	OC5
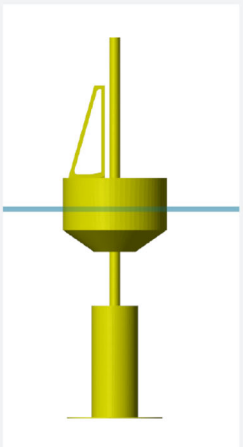	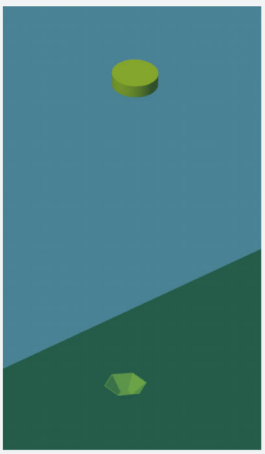	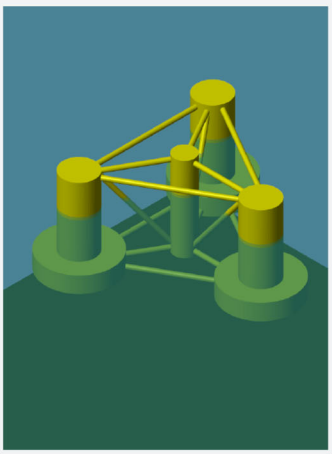
Float diameter = 20.0 m *Float mass = 1.86x10⁶ kg* *Float height = 14.2 m* *Spar diameter = 18.28 m* *Spar mass = 1.42x10⁶ kg* *Spar height = 73.2 m* *PTO damping = 2.69x10⁶ Ns/m*	*Float diameter = 1.83 m* *Float mass = 1166.0 kg* *Float height = 0.81 m* *Float draft = 0.53 m* *heave plate diameter = 1.47 m* *heave plate mass = 257.8 kg* *heave plate height = 0.54 m* *PTO stiffness = 300 N/m* *PTO damping = 10,000 Ns/m*	*Offset column diameter = 12 m* *Lower base column diameter = 24 m* *mass = 1.07x10⁷ kg* *height = 32 m* *Draft = 20 m*

Fig. 4 WEC-Sim model properties of LUPA, miniWEC, and OC5

4.2.1 LUPA

The open-source Laboratory Upgrade Point Absorber (LUPA) WEC was designed and built at Oregon State University. LUPA is an open-source point absorber WEC, which generates power through the relative displacement between the float and spar. LUPA's modular design provides opportunities to test hull geometries, system operation degrees of freedom, PTO control system configurations, and mooring impacts. LUPA has a diameter of 1 m for the laboratory-size device yet, in the simulations for this upsampling methodology, we use the 20-m field-size LUPA. Experimental validation for the numerical models of LUPA is underway and more details on LUPA's design can be found in Bosma et al. (2021).

4.2.2 MiniWEC

The miniWEC is a 2-m field demonstration point absorber developed by University of Washington's Applied Physics Laboratory (APL) funded by Naval Facilities Engineering Command (NAVFAC). MiniWEC generates power, though the tension created between the buoyant surface float and subsurface heave plate. Early field tests with the miniWEC focused on characterizing the hydrodynamics of the WEC, particularly the fluid–structure interactions of heave plates (Brown and Thomson 2016; Brown et al. 2018). Later studies included active control demonstrations and heave plate geometry investigations (Rosenberg et al. 2018; Rusch 2021).

4.2.3 OC5 semisubmersible platform

The third case study is the offshore code comparison, collaboration, continued with correlation (OC5) DeepCwind semisubmersible platform for floating offshore wind turbines (Robertson et al. 2015, 2017; Popko et al. 2018; Srinivas et al. 2023). The Offshore Code Comparison Collaboration (OC3) and extensions including the OC5 are developed under the IEC Technology Collaboration Program (TCP) under the IEC Wind TCP Task 23 and Task 30 (IEC 2023). Extensive effort has been made to analyze and validate the hydrodynamic loads on the semisubmersible cylinders without a wind turbine (Robertson et al. 2015, 2017; Popko et al. 2018; Srinivas et al. 2023). The full-scale platform has a radius of approximately 29-m with a 20-m draft (Robertson et al. 2017). Further studies examine the complete, complex system of the platform and the wind turbine. Unquantified uncertainties of the measurements for the experimental validation resulted in underpredictions in system pitch and loads on OC5 for wave-only cases (Robertson et al. 2015, 2017; Popko et al. 2018; Srinivas et al. 2023). Improving the statistical representation of waves can benefit the wind model by trying to better understand the variability of motions in relation to wave variability.

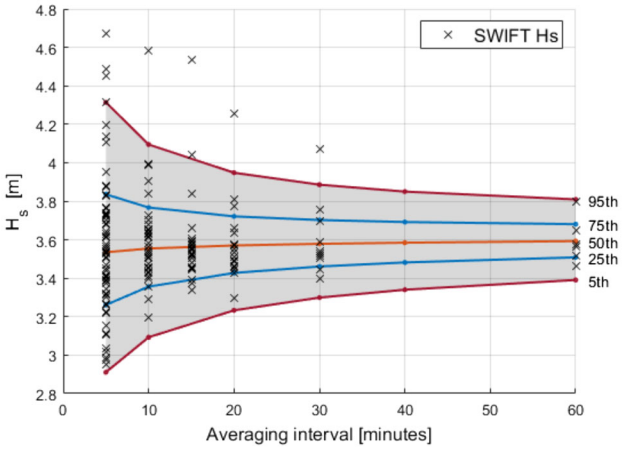

Fig. 5 Significant wave height distribution based on averaging interval. Solid lines identify the different confidence intervals with the shaded area representing the 90th percentile confidence integral

5 Results

To develop confidence in the upsampling methodology, it is important to compare and validate against real-world field measurements. In Figs. 5 and 7, upsampled parametric distributions of significant wave height and maximum wave height are compared to values calculated from high resolution SWIFT data. Figure 5 shows the H_s distribution for the percentiles and averaging intervals. The upsampled probabilistic model calculated from the linear wave simulations (solid lines and shaded area) were generated using the mean H_s from SWIFT data and a variety of averaging intervals. Each vertical spread of SWIFT data points, at each averaging interval, is the H_s calculated based on the specified averaging interval. As the averaging interval increases, the number of representative Hs values decreases.

The SWIFT H_s values fit the probabilistic model in Fig. 5 well with most points falling between the 5th and 95th percentile. The SWIFT data follows the same trend as the probabilistic model, where the variability decreases as the averaging interval increases. The 5-min averaging interval has outliers which comprise of 4.2% of the representative values; which fits within the 95th percentile expectations. The 30-min averaging interval only has one outlier but accounts for 8.3% of the values.

Figure 6 shows the probability density of the unscaled H_s distribution generated from the probabilistic model. Visually, it is apparent that the significant wave height has much larger variability and heavier distribution tails when using a shorter averaging interval. The longer 60-min averaging interval tends to smooth out the variability and reduce the distribution of representative H_s values. There is also a slight shift of the distributions as averaging interval increases. The

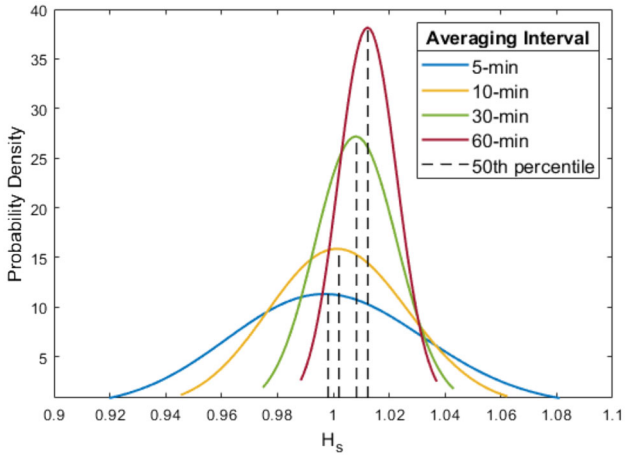

Fig. 6 Probability densities of significant wave heights calculated with increasing averaging intervals

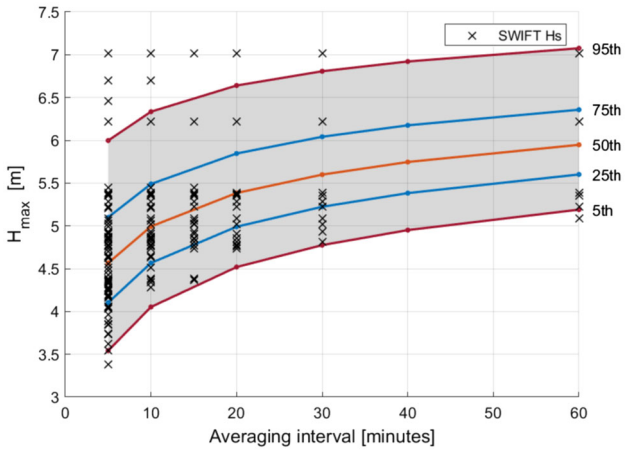

Fig. 7 Maximum wave height distribution based on averaging interval. Solid lines identify the different confidence intervals with the shaded area representing the 90th percentile confidence integral

differences in 50th percentile probability densities are small in Fig. 6 but will increase as the distribution scales with H_s.

The distribution of the upsampled maximum wave height is shown in Fig. 7. Here, the distribution does not trend towards the 50th percentile as the averaging interval increases. However, the variability of $H_{\max}$ is still larger for the 5-min interval compared to the 60-min interval. Adding SWIFT data to the distribution continues to display agreement between the data and the model. The 5-min interval has more outliers than in Fig. 5 but only represents 7% of the $H_{\max}$. The probability densities of $H_{\max}$ in Fig. 8 are more skewed to the right as the averaging interval increases. Figure 8 also displays the unscaled broadness of the 5-min averaging interval. The 5-min averaging interval under predicts the larger $H_{\max}$ values but represents a broader range of $H_{\max}$ values.

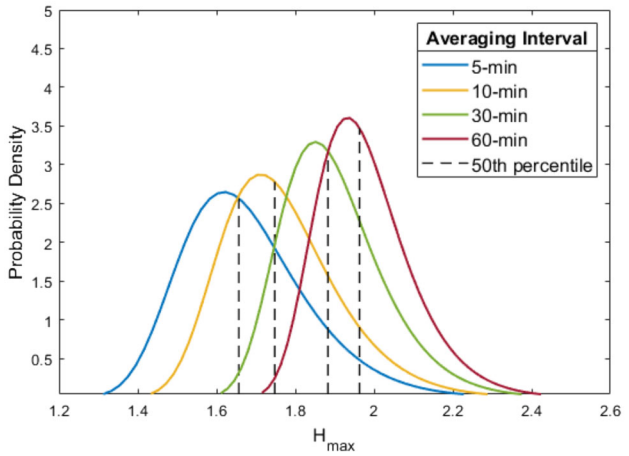

Fig. 8 Probability densities of maximum wave heights calculated with increasing averaging intervals

5.1 Numerical implementation and power assessment

The first two case studies (LUPA and MiniWEC) use the most frequent sea state at PacWave, $H_s = 3$ m and $T_p = 11$ s [54], and the RAS method to generate the respective free-surface time series, $\eta(t)$. RAS time series generated using a representative H_s value for a specified percentile is identified by specific seed numbers. Figures 9 and 10 show the H_s and $H_{\max}$ distributions calculated from the generated time series for seed 221112. The distribution in Fig. 9 follows the same distribution, as shown in Fig. 5. The probabilistic model for $H_{\max}$ in Fig. 10 follows the general shape of the $H_{\max}$ distribution, as shown in Fig. 7. However, it should be noted that due to the randomness of the generation methodology, a time series from a single seed will not generate the exact probabilistic $H_{\max}$ model across all averaging intervals (shown in Fig. 7). All cases were simulated in WEC-Sim (Ruehl et al. 2022) with the same time series scaled based on the wave conditions described for each case.

For the third case study (OC5), with a focus on quantifying the impact of upsampling on surge forces acting on the platform, a larger sea state was used. PacWave is also chosen as a reference in this case for an extreme sea state, where $H_s = 8$ m and $T_p = 11$ s.

5.1.1 LUPA

The average power generated from LUPA is shown in Fig. 11. The distribution of average power over the different averaging intervals follows the H_s distributions from the probabilistic model. The 5th and 95th percentile intervals decrease significantly for the 18-min averaging interval following a gradual shift towards the 50th percentile average power. The 95th confidence interval for the 3-min averaging

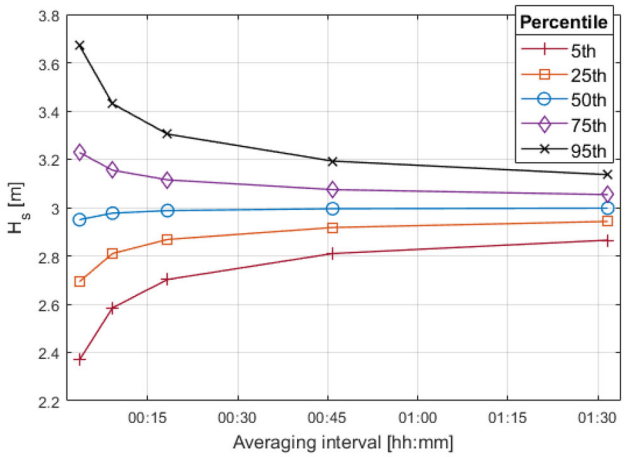

Fig. 9 Significant wave height distribution of free-surface time series input into WEC-Sim based on averaging interval. Solid lines identify the representative H_s of a given percentile

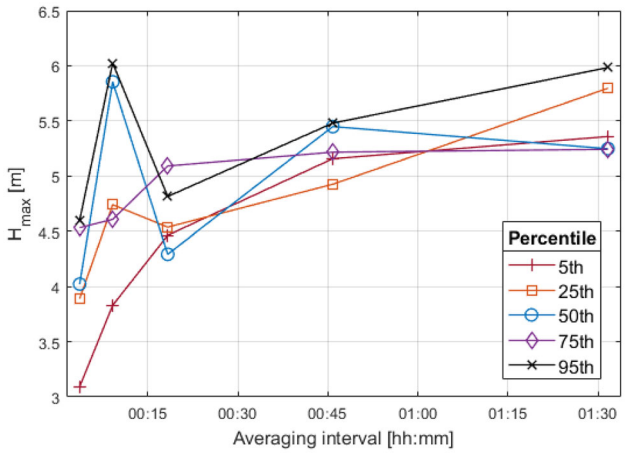

Fig. 10 Maximum wave height distribution of free-surface time series input into WEC-Sim based on averaging interval. Solid lines identify the representative $H_{\max}$ of a given percentile

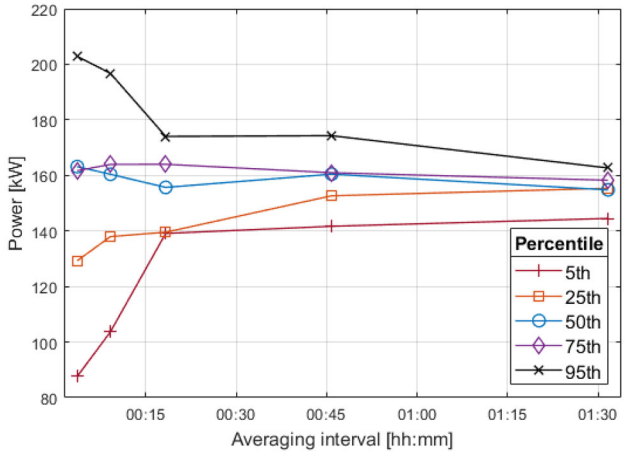

Fig. 11 Average power distribution from LUPA simulations of given averaging intervals. Solid lines identify the representative average power of a given percentile

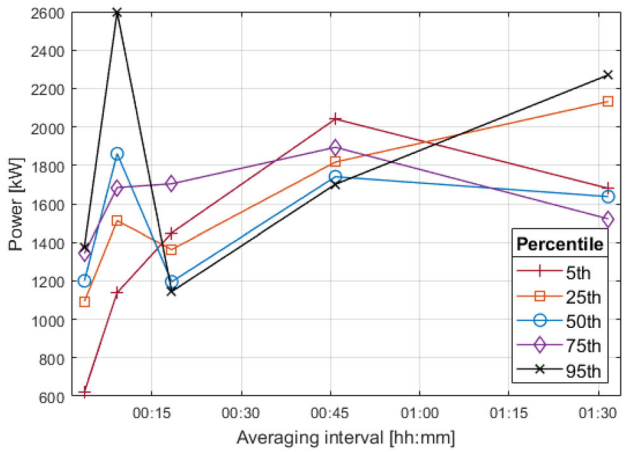

Fig. 12 Maximum power distribution from LUPA simulations of given averaging intervals

interval has a spread of 87.2 kW which is 130% larger than the spread of average power for the 90-min averaging interval—which would have significant implications for various WEC end users.

The max power distribution in Fig. 12 follows the same trend as the probabilistic model. The 9-min averaging interval has a large max power for the 95th percentile which corresponds to the $H_{\max}$ for the 95th percentile in Fig. 10. Noteworthy is that the 3-min averaging interval underpredicts the maximum power values compared to the larger averaging intervals. However, the variability of maximum power is larger for the 3-min averaging interval range from 623 to 1375 kW, while the maximum values for the 90-min interval range from 1521 to 2270 kW with power spreads of 752 and 749 kW, respectively.

The empirical cumulative distribution function (CDF) is also analyzed. For clarity, only the 3-min and 90-min averaging intervals are shown in Fig. 13. Each averaging interval has multiple lines representing the different percentiles used in the study. The spread of probability distributions for the 3-min averaging interval is much wider and is consistent with the increased variability of very-short averaging intervals. It shows a higher probability of a wider range of maximum power values, and an underprediction of maximum power values.

Figure 13 offers an additional display of the power distribution for different averaging periods. The maximum values found in Fig. 13 are also the maximum power values shown in Fig. 12. When moving away from the largest power values, even at the $90th$ percentile, the range of power for the 3-min interval is significantly larger than the 90-min interval, with power spreads of 283 and 56 kW, respectively.

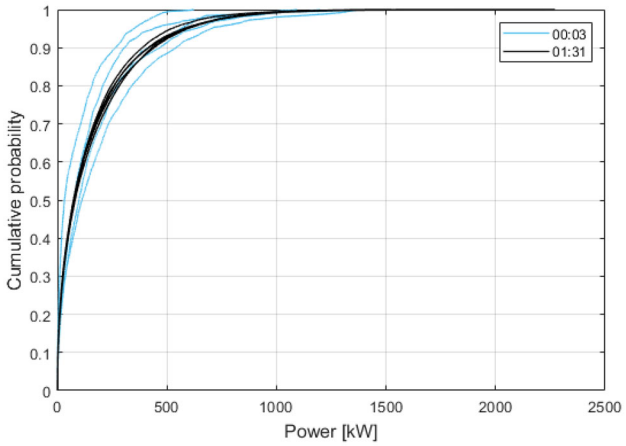

Fig. 13 Empirical cumulative distribution function of power generated by LUPA for different averaging intervals of given percentiles

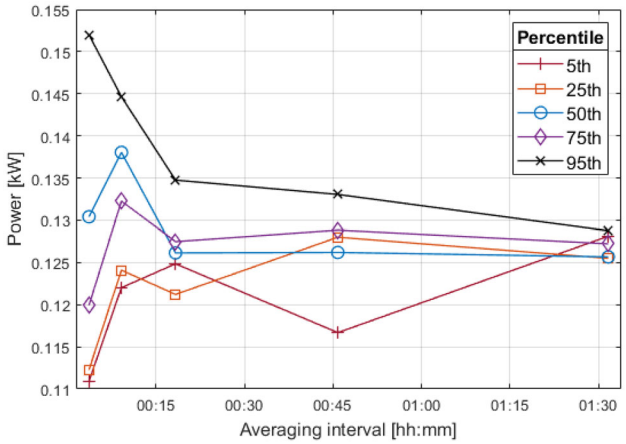

Fig. 14 Average power distribution from miniWEC simulations of given averaging intervals

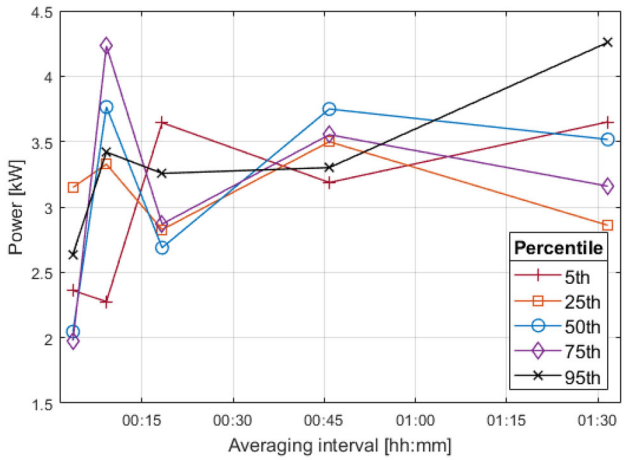

Fig. 15 Max power distribution from miniWEC simulations of given averaging intervals

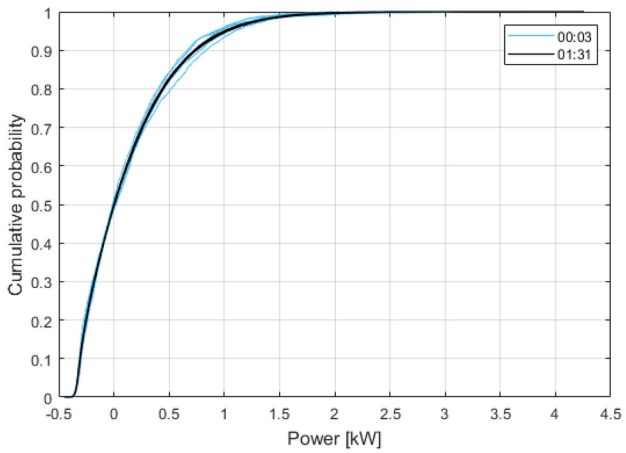

Fig. 16 Empirical cumulative distribution function of power generated by the MiniWEC for different averaging intervals surge of given percentiles

5.1.2 MiniWEC

The average power generated from miniWEC is shown in Fig. 14. First, it is interesting to note that the trends are different than for LUPA on the exact same time series. This indicates the the MiniWEC may be a more non-linear WEC conversion technology. The 95th confidence interval for the 3-min averaging interval has a spread of 79.3 W, which is 171% larger than the spread of average power for the 90-min averaging interval.

Interestingly, the max power distribution in Fig. 15 does not follow the trend found in Fig. 6. The 3-min averaging interval under-predicts the maximum power values compared to the larger averaging intervals. Other outliers are found for the 45- and 130-min averaging intervals. Excluding those values, an increase in maximum power from the 3- to 130-min averaging interval is present. However, the variability of maximum power is larger for the 130-min averaging interval range from 3.2 to 4.2 kW, while the maximum values for the 3-min interval range from 1.6 to 2.1 kW with power spreads of 1 and 0.5 kW, respectively. It should be noted that max power is not a very stable metric and is highly variable to single measurements.

The empirical CDF is shown in Fig. 16. 90% of the power generated from the miniWEC is under 50 kW which is to be expected from a small WEC. The 130-min averaging interval shows a large spread in Fig. 16 too, but as mentioned, this is due to the maximum power outlier.

5.1.3 OC5

The third case study assesses the impact of temporal upsampling on the forces, and associated motions, acting on the OC5 floating offshore wind platform. A larger sea state was chosen for this case study due to the size of the OC5 platform.

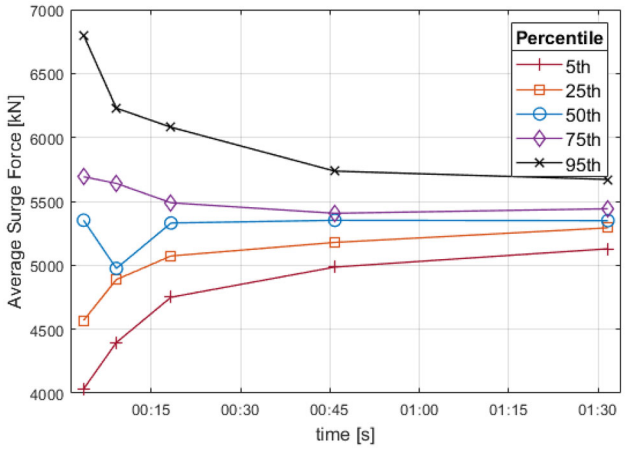

Fig. 17 Average surge force from OC5 simulations of given averaging intervals

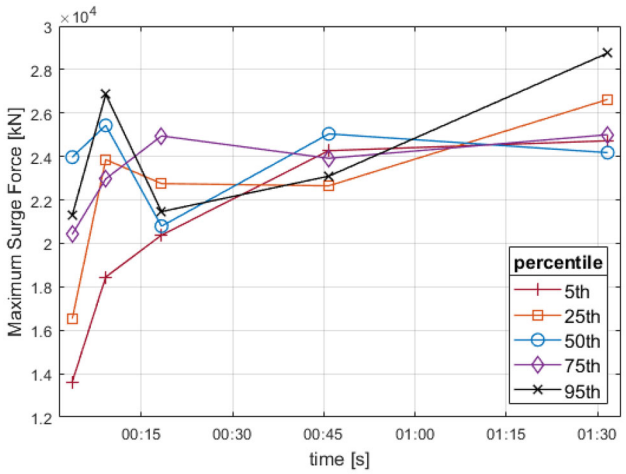

Fig. 18 Maximum surge force from OC5 simulations of given averaging intervals

The surge force acting on the platform is shown in Figs. 17 and 18 for the time series of different wave height percentiles and averaging intervals. The distribution of the surge force follows the H_s distributions from the probabilistic model. The 5th and 95th percentile intervals in Fig. 16 decrease gradually in Fig. 17 as the averaging interval increases, again resembling the average H_s distribution. The 95th confidence interval for the 3-min averaging interval has a spread of 2800 kN which is 134% larger than the spread of average power for the 90-min averaging interval. Again, this has significant implications for the design and build for the forecasting the impacts on offshore floating bodies.

The max surge force distribution in Fig. 18 also follows the same trend as the probabilistic model in Fig. 7. The 3-min averaging interval continues to under-predict the maximum values compared to the larger averaging intervals. The variability of the maximum surge force is larger for the 3-min averaging interval range from 13,625 to 23,970 kN, while the

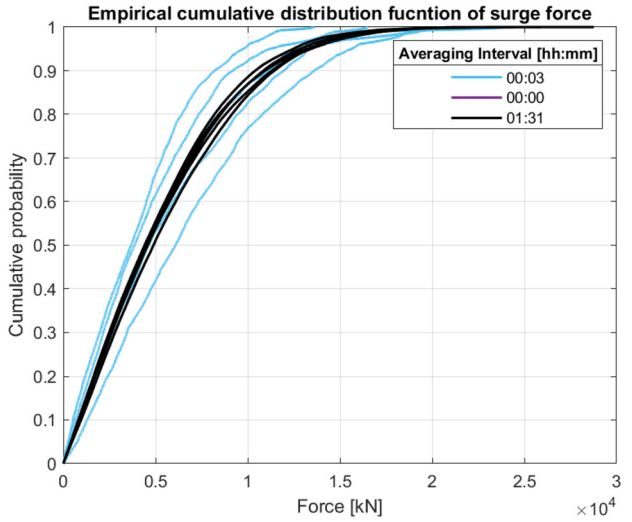

Fig. 19 Empirical cumulative distribution function of surge force acting on OC5 for different averaging intervals of given percentiles

maximum values for the 90-min interval range from 24,177 to 28,763 kN with the forces spreading 10,345 and 4586 kN, respectively.

The empirical CDF is shown in Fig. 19. Looking at the 90th percentile, the range of power for the 3-min interval is significantly larger than the 90-min interval, with surge forces spreads of 5505 and 1029 kN, respectively.

6 Discussion

Time domain predictions of power production and hydrodynamic forcing in very-short averaging intervals require high temporal wave inputs to accurately simulate the variability in hydrodynamic models with high temporal resolutions (10s of Hz). This research demonstrates that wave parameters, that are developed with very-short but realistic averaging intervals, have significantly increased variability (when compared against status quo of 1–3 h data) and subsequently increases the variability in power and forces in simulations.

From a purely wave resource condition perspective, variability of significant and maximum wave heights are influenced heavily by the averaging interval (as shown in Figs. 5, 6, 7 and 8). Variability increased significantly for smaller averaging intervals, representing a much broader range of wave conditions at the WEC. Looking at Figs. 5 and 7, the SWIFT data recordings fit the probabilistic model well with outliers generally following the statistical distributions. As shown, the true variability of wave conditions is obscured if using averaging intervals over 30 min, leading to under representations of the 5th and 95th percentile significant wave heights. This has distinct implications on offshore floating structural design and electrical system power integration.

Further work is needed to explore the impact other parameters have on the variability of the free-surface time series, specifically the peak enhancement factor and wave energy period. Energy period is preferred to peak period by representing the full distribution of variance across the frequencies of a wave spectrum. Although peak period was discussed in previous sections and is an input for the JONSWAP spectrum, it corresponds to the maximum variance density in the spectrum and is independent from the full distribution (Robertson 2017). Peak periods use in marine energy modeling is extensive but is not the metric used to characterize wave conditions set by the International Electrotechnical Commission (IEC 2012).

By investigating three cases of WECs and offshore wind technology, the upsampling process demonstrated the increase in variability of hydrodynamic forces and performance metrics for very-short averaging intervals. Based on LUPA's power generation, power distributions may not change significantly starting at averaging intervals above 20 min, but had significant variability and spread for shorter averaging intervals.

It is worth noting that this study only uses a single random seed from the 10-million-member ensemble (specifically representing the 5th/25th/50th/75th/95th percentiles of the wave parameters). Using slightly different percentiles would require a different seed, which would alter the outputs of the WEC-Sim simulations in a non-linear fashion. It is anticipated that analyzing a larger number of seeds for each simulation, would result in the output value distributions resembling the H_s distribution more closely.

For the outputs for LUPA and the OC5 platform, the $H_{\max}$ distribution clearly demonstrated influence over the maximum power and force of the technology. As a result, simulating offshore technology for very-short time periods and associated averaging intervals may under-predict maximum values. This is expected and indicates that longer time averaging intervals using both DAS and RAS might be sufficient for prediction of extreme loads.

As discussed in Mérigaud and Ringwood (2018), choosing the method for modeling wave inputs depends on the intended objective of the simulations. In their study, they compare the power outputs from the deterministic amplitude scheme (DAS) and random amplitude scheme (RAS) methods for different numerical setups. RAS is encouraged in all strongly nonlinear cases and for finite durations for linear and weakly nonlinear cases. In this study, the RAS upsampling methodology provided wave inputs with accurate statistics for a range of percentiles which provides a more detailed understanding of the wave field and WEC performance for very-short averaging intervals.

For end-user applications, such as WEC-powered remote micro-grids, statistically accurate power predictions are required for very-short averaging intervals. Using the developed RAS upsampling method will provide a better representation of the true variability and the associated needs of power system.

7 Conclusion

As offshore renewable energy becomes more prevalent, the need for accurate wave predictions is crucial in the performance assessment, survival, and operation of the technology. Publicly accessible wave measurements from buoys or wave models provide data with low temporal resolution (1 or 3 h)—which is not sufficient for modeling the natural variability of the ocean for floating body dynamics. Accurate wave predictions that capture the stochasticity of the waves require higher temporal resolution. This study develops and demonstrates an upsampling methodology that better represents the real variability of wave conditions and uses them as input into time-domain models by generating free surface time series with the random amplitude scheme.

The increased variability of wave conditions with high-temporal-resolution data has important implications for the design and operation of wave energy converters. Accurately modeling and predicting the variability of ocean waves is essential for ensuring the reliable and efficient operation of these offshore systems and the associated end-users of the generated offshore renewable energy. In this study, variability of wave parameters was analyzed against real data by decreasing the averaging interval as small as possible while maintaining statistical accuracy. Real-world field data sampled at different averaging intervals matched well within the 95% confidence intervals of the probabilistic model for significant wave height and maximum wave height. Significant wave height has larger variability and heavier distribution tails using shorter averaging intervals. Maximum wave height also has larger variability with shorter averaging intervals but under-represents the largest values.

Increased temporal resolution free surface time series, generated using the probabilistic models, maintained the accurate stochastic representation of different percentiles of wave conditions. These time series were then employed to investigate the variability of power and hydrodynamic forces on WECs and platforms. In the three cases, variability of power and forces show the increase in variability within the 95% confidence intervals for the small averaging intervals, demonstrating the effectiveness of the upsampling methodology for different types of offshore applications.

LUPA simulations show an increase in variability for very-short averaging intervals and a steep decline in variability with averaging intervals of 18-min and higher. Power distributions from the MiniWEC varied from the other cases. Nonlinearities in the system affected the power distributions due to the small size of the WEC. The surge forces acting on

the OC5 in extreme sea conditions produced distributions following significant wave height and maximum wave height, even with a much larger natural period.

The upsampling methodology presented in this study provides a promising solution for predicting power and hydrodynamic forcing for WECs and offshore wind technology in very-short averaging intervals with low computational cost.

This study highlights the importance of statistical representation for ocean waves and the need for accurate wave predictions for marine energy applications. The use of high-temporal-resolution data can lead to more reliable and effective operation and monitoring of wave energy converters, providing a framework for future grid-integration. This study highlights the importance of modeling free surface time series with large variability and the effect the wave variability has on WEC performance. Further research is necessary to investigate the feasibility of standardized framework for this methodology for future WEC integration.

Author Contributions **HM:** investigation, methodology, software, data curation, original draft preparation. **PB:** investigation, methodology, software, data curation, reviewing and editing. **BDP:** reviewing and editing. **BR:** conceptualization, resources, funding acquisition, reviewing and editing.

Funding This material is based upon work supported by the U.S. Department of Energy, Office of Science, Office of Energy Efficiency and Renewable Energy under Award Number DE-EE0009445.

Availability of data and materials Data and materials available on request. Data will be publicly available with future publications.

Declarations

Conflict of interest The authors declare that they have no known competing financial interests or personal relationships that could have appeared to influence the work reported in this paper.

Ethical approval Not applicable.

References

Alves M (2016) Frequency-domain models. In: Numerical Modelling of Wave Energy Converters. Academic Press, pp 11–30

Ancellin M, Dias F (2019) Capytaine: a Python-based linear potential flow solver. J Open Source Softw 4(36):1341. https://doi.org/10.21105/joss.01341. Accessed 02 Nov 2022

Australia Ocean Data Network (2023) AODN Open Access to Ocean Data. https://portal.aodn.org.au/. Accessed 20 Jan 2023

Babarit A, Delhommeau G (2015) Theoretical and numerical aspects of the open source BEM solver NEMOH. In: Presented at the 11th European Wave and Tidal Energy Conference (EWTEC2015). https://hal.science/hal-01198800. Accessed 11 Apr 2023

Babarit A, Hals J, Muliawan MJ, Kurniawan A, Moan T, Krokstad J (2011) Numerical benchmarking study of a selection of wave energy converters. https://doi.org/10.1016/j.renene.2011.10.002

Bosma B, Beringer C, Leary M, Robertson B (2021) Design and modeling of a laboratory scale WEC point absorber. In: Proc. of the 14th European Wave and Tidal Energy Conference, Plymouth, UK

Bosma B, Zhang Z, Brekken TKA, Ozkan-Haller HT, McNatt C, Yim SC (2012) Wave energy converter modeling in the frequency domain: A design guide. In: 2012 IEEE Energy Conversion Congress and Exposition (ECCE). IEEE, Raleigh, pp 2099–2106. https://doi.org/10.1109/ECCE.2012.6342553

Brown A, Thomson J (2016) Phase-resolved heave plate dynamics. In: Proceedings of the 4th Marine Energy Technology Symposium

Brown A, Thomson J, Rusch C (2018) Hydrodynamic coefficients of heave plates, with application to wave energy conversion. IEEE J Ocean Eng 43(4):983–996. https://doi.org/10.1109/JOE.2017.2762258. Accessed 13 Jan 2023

California SD (2023) Coastal Data Information Program (CDIP). https://cdip.ucsd.edu/m/. Accessed 01 Nov 2022

Department of Energy Water Power Technology Office (2023) DOE's Water Power Technology Office's (WPTO) US Wave dataset. https://registry.opendata.aws/wpto-pds-us-wave. Accessed 01 Nov 2022

Fairley I, Smith HCM, Robertson B, Abusara M, Masters I (2017) Spatio-temporal variation in wave power and implications for electricity supply. Renew Energy 114:154–165. https://doi.org/10.1016/j.renene.2017.03.075. Accessed 13 Oct 2022

Fusco F, Ringwood JV (2010) Short-term wave forecasting for real-time control of wave energy converters. IEEE Trans Sustain Energy 1(2):99–106. https://doi.org/10.1109/TSTE.2010.2047414

Gioia DG, Pasta E, Brandimarte P, Mattiazzo G (2022) Data-driven control of a pendulum wave energy converter: a Gaussian process regression approach. Ocean Eng 253:111191. https://doi.org/10.1016/j.oceaneng.2022.111191. Accessed 30 Sep 2022

Group TW (1988) The WAM Model-A third generation ocean wave prediction model. J Phys Oceanogr 18(12):1775–1810. https://doi.org/10.1175/1520-0485(1988)018<1775:TWMTGO>2.0.CO;2 (**Publisher: American Meteorological Society Section: Journal of Physical Oceanography**)

Hasselmann K, Barnett TP, Bouws E, Carlson H, Cartwright DE, Enke K, Ewing JA, Gienapp A, Hasselmann DE, Kruseman P (1973) Measurements of wind-wave growth and swell decay during the joint North Sea wave project (jonswap). Ergaenzungsheft zur Deutschen Hydrographischen Zeitschrift, Reihe A

IEC (2012) International Electrotechnical Commission TS 62600-100. https://webstore.iec.ch/publication/7241. Accessed 20 Nov 2022

IEC (2015) International Electrotechnical Commission TS 62600-101. https://webstore.iec.ch/publication/22593. Accessed 20 Nov 2022

IEC (2023) International Electrotechnical Commission Wind TCP task 30. https://iea-wind.org/task30/. Accessed 11 Feb 2023

Medium-Range Weather Forecasts EC (2023) European Center for Medium-Range Weather Forecast. https://www.ecmwf.int/en/forecasts/datasets

Mérigaud A, Ringwood JV (2018) Free-surface time-series generation for wave energy applications. IEEE J Ocean Eng 43(1):19–35. https://doi.org/10.1109/JOE.2017.2691199 (**Conference Name: IEEE Journal of Oceanic Engineering**)

National Oceanic and Atmospheric Administration (2022) NOAA National Data Buoy Center. https://www.ndbc.noaa.gov/. Accessed 01 Nov 2022

OceanSITES (2023) OceanSITES: taking the pulse of the global ocean. http://www.oceansites.org/. Accessed 20 Jan 2023

PacWave (2022) PacWave—testing wave energy for the future. https://pacwaveenergy.org/. Accessed 26 Oct 2022

Peña-Sanchez Y, Mérigaud A, Ringwood JV (2020) Short-term forecasting of sea surface elevation for wave energy applications: the autoregressive model revisited. IEEE J Ocean Eng 45(2):462–471. https://doi.org/10.1109/JOE.2018.2875575 (**Conference Name: IEEE Journal of Oceanic Engineering**)

Pierson Jr WJ, Moskowitz L (1964) A proposed spectral form for fully developed wind seas based on the similarity theory of s.a. kitaigorodskii. J Geophys Res (1896-1977) 69(24):5181–5190. https://doi.org/10.1029/JZ069i024p05181. https://onlinelibrary.wiley.com/doi/pdf/10.1029/JZ069i024p05181

Popko W, Huhn ML, Robertson A, Jonkman J, Wendt F, Müller K, Kretschmer M, Vorpahl F, Hagen TR, Galinos C, Le Dreff J-B, Gilbert P, Auriac B, Víllora FN, Schünemann P, Bayati I, Belloli M, Oh S, Totsuka Y, Qvist J, Bachynski E, Sørum SH, Thomassen PE, Shin H, Vittori F, Galván J, Molins C, Bonnet P, Zee T, Bergua R, Wang K, Fu P, Cai J (2018) Verification of a numerical model of the offshore wind turbine from the alpha ventus wind farm within oc5 phase III. In: Volume 10: ocean renewable energy. American Society of Mechanical Engineers, Madrid, pp 010-09056. https://doi.org/10.1115/OMAE2018-77589

Reikard G, Robertson B, Bidlot J-R (2015) Combining wave energy with wind and solar: short-term forecasting. Renew Energy 81:442–456. https://doi.org/10.1016/j.renene.2015.03.032. Accessed 13 Oct 2022

Reikard G, Robertson B, Buckham B, Bidlot J-R, Hiles C (2015) Simulating and forecasting ocean wave energy in western Canada. Ocean Eng 103:223–236. https://doi.org/10.1016/j.oceaneng.2015.04.081. Accessed 30 Dec 2022

Reikard G, Rogers WE (2011) Forecasting ocean waves: comparing a physics-based model with statistical models. Coast Eng 58(5):409–416. https://doi.org/10.1016/j.coastaleng.2010.12.001. Accessed 18 Oct 2022

Ren Y, Suganthan PN, Srikanth N (2015) Ensemble methods for wind and solar power forecasting—a state-of-the-art review. Renew Sustain Energy Rev 50:82–91. https://doi.org/10.1016/j.rser.2015.04.081. Accessed 24 Oct 2022

Ricci P (2016) Time-domain models. Numer Model Wave Energy Convert:31–66. https://doi.org/10.1016/B978-0-12-803210-7.00003-7

Ricci P, Saulnier J-B, Falcaõ AFdO, Pontes MT (2008) Time-domain models and wave energy converters performance assessment. In: Volume 6: Nick Newman Symposium on marine hydrodynamics; Yoshida and Maeda special symposium on ocean space utilization; special symposium on offshore renewable energy. ASMEDC, Estoril, pp 699–708. https://doi.org/10.1115/OMAE2008-57642

Robertson AN, Wendt FF, Jonkman JM, Popko W, Vorpahl F, Stansberg CT, Bachynski EE, Bayati I, Beyer F, Vaal JB, Harries R, Yamaguchi A, Shin H, Kim B, Zee T, Bozonnet P, Aguilo B, Bergua R, Qvist J, Qijun W, Chen X, Guerinel M, Tu Y, Yutong H, Li R, Bouy L (2015) OC5 Project Phase I: validation of hydrodynamic loading on a fixed cylinder. International Ocean and Polar Engineering Conference, vol all days. https://onepetro.org/ISOPEIOPEC/proceedings-pdf/ISOPE15/All-ISOPE15/ISOPE-I-15-116/1338148/isope-i-15-116.pdf

Robertson AN, Wendt F, Jonkman JM, Popko W, Dagher H, Gueydon S, Qvist J, Vittori F, Azcona J, Uzunoglu E, Soares CG, Harries R, Yde A, Galinos C, Hermans K, Vaal JB, Bozonnet P, Bouy L, Bayati I, Bergua R, Galvan J, Mendikoa I, Sanchez CB, Shin H, Oh S, Molins C, Debruyne Y (2017) Oc5 project phase II: validation of global loads of the deepcwind floating semisubmersible wind turbine. Energy Procedia 137:38–57. https://doi.org/10.1016/j.egypro.2017.10.333 . Accessed 13 Jan 2023

Robertson B (2017) Wave energy assessments: quantifying the resource and understanding the uncertainty. In: Yang Z, Copping A (eds) Marine Renewable Energy: Resource Characterization and Physical Effects. Springer, pp 1–36.https://doi.org/10.1007/978-3-319-53536-4_1

Robertson B, Bailey H, Leary M, Buckham B (2021) A methodology for architecture agnostic and time flexible representations of wave energy converter performance. Appl Energy 287:116588. https://doi.org/10.1016/J.APENERGY.2021.116588 (**Publisher: Elsevier**)

Rojas A, Rousan T (2017) Microgrid control strategy: derived from stakeholder requirements analysis. IEEE Power Energy Mag 15(4):72–79. https://doi.org/10.1109/MPE.2017.2690520 (**Conference Name: IEEE Power and Energy Magazine**)

Rosenberg B, Mundon T, Cavagnaro R, Rusch C, Thomson J, Polagye B (2018) Development and field testing of PTO control strategies for two-body flexibly connected WECs. In: Proceedings of the 6th Marine Energy Technology Symposium

Ruehl K, Keester A, Ströfer CAM, nathanmtom, Topper M, Lawson M, dforbush2, Ling BA, jtgrasb, j-vanrij, Sal, jhbates, Ogden D, Nguyen L, Jeffalo1, Leon J, sedwardsand, Alves EF, crobarcro, emiliofa, ratanakso, Rshid A, Aquaharmonics, Sauer F, Ancellin M, NREL-Jim-Mcally, SiHeTh, gparisella, Hall M (2022) yuyihsiang: WEC-Sim/WEC-Sim: WEC-Sim v5.0.1. Zenodo. https://doi.org/10.5281/zenodo.7121186. https://zenodo.org/record/7121186. Accessed 23 May 2023

Rusch C (2021) Scaling of point-absorber wave energy converter hydrodynamics. Doctoral dissertation, University of Washington

Said HA, Ringwood JV (2021) Grid integration aspects of wave energy-overview and perspectives. IET Renew Power Gener 15(14):3045–3064. https://doi.org/10.1049/rpg2.12179. https://onlinelibrary.wiley.com/doi/pdf/10.1049/rpg2.12179. Accessed 18 May 2023

Saulnier J-B, Ricci P, Clément AH, Falcaõ AFdO (2009) Mean power output estimation of wecs in simulated sea. In: Proceedings of The 8th European Wave and Tidal Energy Conference (EWTEC) 2009, vol 710. Uppsala

Srinivas A, Robertson B, Gadasi JB, Simpson BG, Lomónaco P, Ilzarbe JMB (2023) Impact of limited degree of freedom drag coefficients on a floating offshore wind turbine simulation. J Mar Sci Eng 11(1):139. https://doi.org/10.3390/jmse11010139. Accessed 31 Jan 2023

team TS (2018) Swan user manual. Swan cycle III version 41.20a

Thomson J (2012) Wave breaking dissipation observed with "swift" drifters. J Atmos Ocean Technol 29(12):1866–1882. https://doi.org/10.1175/JTECH-D-12-00018.1. Accessed 26 Oct 2022

Thomson J, Brown A, Ozkan-Haller T, Ellenson A, Haller M (2016) Extreme conditions at wave energy sites. In: Proceedings of the 4th Marine Energy Technology Symposium

Tobergte DR, Curtis S (2013) WAMIT user manual 53(9):1689–1699. https://doi.org/10.1017/CBO9781107415324.004

Tolman HL (2009) User manual and system documentation of WAVEWATCH III TM (version 3.14). Technical note, MMAB Contribution, vol 276, no 220

Tucker MJ, Challenor PG, Carter DJT (1984) Numerical simulation of a random sea: a common error and its effect upon wave group statistics. Appl Ocean Res 6(2):118–122